JOINT EUROPEAN TORUS JET

JET–P(93)53

H.D. Falter, D. Ciric, P. Massmann, A. Cardella, M. Akiba

Testing of Plasma Facing Materials for Divertors in the JET Neutral Beam Test Bed

Testing of Plasma Facing Materials for Divertors in the JET Neutral Beam Test Bed

H.D. Falter, D. Ciric, P. Massmann, A. Cardella[1], M. Akiba[2]

JET-Joint Undertaking, Culham Science Centre, OX14 3DB, Abingdon, UK

[1]The NET Team, Max-Planck Institute fuer Plasma Physik,
Garching bei Mtinchen, Germany.
[2]NBI Heating Laboratory Naka Fusion Research Establishment, JAERI,
Naka-machi, Naka-gun, Ibaraki-ken, Japan.

July 1993

Testing of Plasma Facing Materials for Divertors in the JET Neutral Beam Test Bed

H D Falter[1], D Ciric[1], P Massmann[1], A Cardella[2], M Akiba[3]

[1]) JET Joint Undertaking Abingdon, OXON, OX14 3EA, England
[2]) THE NET TEAM, Max-Planck Institut für Plasma Physik, Boltzmannstrasse 2, D 8046 Garching bei München, Germany
[3]) NBI Heating Laboratory Naka Fusion Research Establishment, JAERI, 801 -1 Naka-machi, Naka-gun, Ibaraki-ken, 311-01 Japan

ABSTRACT

Flat Beryllium tiles brazed to actively cooled CuCrZr withstand power densities up to 17 MW/m^2. Tiles with 2 mm thickness have been cycled for 1000 pulses at power densities between 12 and 14 MW/m^2.

Flat CFC tiles brazed to OFHC copper failed at power densities of 13 MW/m^2 with long (10 s) pulses. The fault developed from an area which showed signs of overheating from the start of the test and led to a complete detachment of one tile. For shorter pulse duration (2.5 s) higher power densities (17 MW/m^2) could be applied.

CFC cubes brazed around a central cooling pipe (monoblocks) have been tested to 15 MW/m^2. The power density was limited by the peak surface temperature of the tiles, which exceeded 1500 - 2000 ^{0}C. None of the tiles failed during the test, but there were considerable temperature variations from tile to tile.

1 INTRODUCTION

The JET Joint European Torus[1] in Culham U.K. operates in a pulsed mode with a pulse duration of up to 60s. The plasma is confined by magnetic fields and heated by the current in the plasma (up to 7 MA). Up to 40 MW of additional power can be supplied by the plasma heating systems. The exhausted power is absorbed in specially designed dumps. Impurities released from the dumps can lead to radiative losses and to dilution of the plasma. Both effects increase with the atomic number Z of the impurity. To minimise plasma contamination, low surface temperatures of the dump plates and a dump surface material with a low atomic number, such as Beryllium or Graphite, are beneficial. Any misalignment of the dump plates will cause localised hot spots and must be avoided.

A so-called "divertor"[2], which separates the dump area from the plasma, is at present being installed into the JET machine. In the divertor a null, or 'X' point is created in the magnetic field at the plasma boundary. Particles leaving the plasma are conducted along the open field lines to a divertor dump hitting it at so called strike points. The peak power density expected at the strike point is of the order of 60 MW/m^2 at a heating power of 40 MW. So-called X events[3], observed in high performance discharges, can result in loss of energy from the plasma and in considerable bursts of higher power densities[4]. Although the average power can be reduced by magnetically sweeping the strike point over the target plate the resulting peak power density is still dangerously close to the performance limit of actively cooled dump plates. It has therefore been decided to use inertial dump plates for the Mark I divertor in JET. It is expected that the power loading on the divertor dump plate can be significantly reduced in advanced divertor concepts[5].

Fig. 1: Plan view of the main test facility

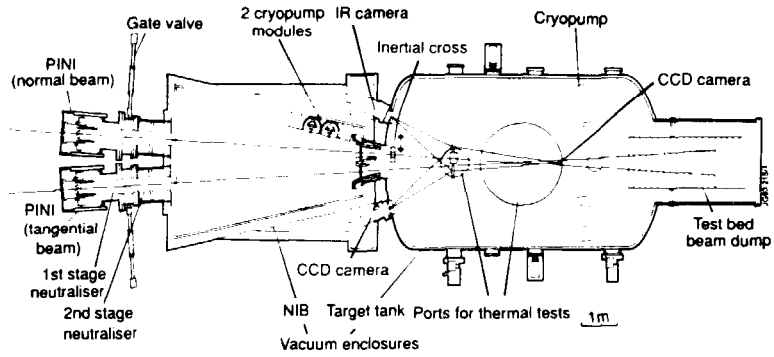

Power densities up to 15 - 20 MW/m^2 can be handled with CFC tiles brazed to a cooled base structure[6] [7]. For the application of this technique in a fusion experiment the peak surface temperature is of crucial importance and in a multi-tile structure such as the divertor the worst tile defines the performance limit. To examine, if these techniques can be used for a JET divertor, tests have been carried out on samples supplied by NET and JAERI. Apart from the power density limit, the reliability of the technique and the variation in surface temperature are of particular interest.

2 TEST FACILITY

All the tests in this report have been performed in the JET Neutral Beam Test Bed; a 10 MW, 160 kV ion beam line system originally used to commission the JET neutral beam injectors (Fig. 1). The main parameters of the Test Bed are shown in Table 1. Tests on CFC components were carried out in the Target Tank. Samples with Beryllium were tested in a second smaller beam line, the so called Beryllium test rig (Fig. 2).

Table 1: Parameters of the JET test facilities

	main test bed	**Be test rig**
heat source	ion beam	
pulse duration	20s	
max. power	2 x 4 MW	2 MW
max. power density	100 MW/m^2 per beam	> 50 MW/m^2
duty cycle	1 : 30	
volume	90m^3	1 m^3
access ports	up to 1500 mm i.d.	400 mm i.d.
vacuum pumping speed	10^6 l/s	200 - 1000 l/s
Cooling loop capacity available for tests:		
water flow rate and pressure head	20 l/s (8 bar) & 100 l/s (4.5bar)	IR. thermal imaging and high resolution CCD cameras
return water pressure	2 bar	
Diagnostics		
thermal diagnostics	> 200 thermocouple channels (40 Hz)	
visual diagnostics	IR. thermal imaging and high resolution CCD cameras	
gas	residual gas analyser and spectrometer	
Shielding	Fully shielded for operation with deuterium beams.	

The Beryllium test rig is a small beam line with a volume of approximately 1 m^3. The whole tank is operated at the pressure required in the plasma source to produce an arc (0.2 - 0.3 Pascal). This reduces considerably the requirement for vacuum pumping speed to less than 1000 l/s. A standard JET beam source (PINI) with a reduced extraction area is used. Power supplies, control & data acquisition, and the cooling loop of the main Test Bed are shared with the main beam line.

Fig. 2: Test facility for Beryllium components.

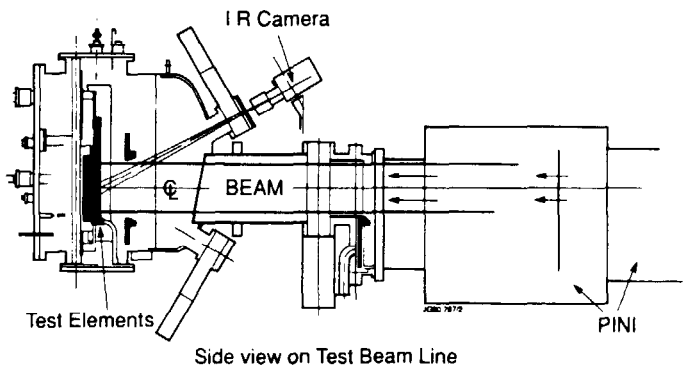

2.1 Diagnostics

- **Surface temperature**: The surface temperature of the test panel is measured with an AGA IR camera. If the design of the test sections allows sufficiently high temperatures, the IR system is calibrated during the radiative cooldown of the panel, when thermal gradients can be neglected. Emissivity and transmission are than set to match the surface temperature of the panel with that measured with a thermocouple inserted into the panel.

- **Panel temperature**: Grounded hot junction CrAl thermocouples are percussion welded into 1.7 mm holes in the case of metal substrates. For CFC substrates 1 mm sheathed thermocouples are pushed and spring loaded into drillings. The thermocouple output is sampled with a rate of approximately 40 Hz.

- **Power density**: The power density is normally measured with water calorimetry and with inertial copper calorimeters. Water flow is measured using Taylor turbine flowmeters installed in the return line of each water channel. The water exit temperature is measured with sheathed CrAl thermocouples sampled at a rate of 6 Hz. The signal level before the pulse is used as a base line. The peak power density p_0 is calculated from the absorbed energy E_{total} using the equation

$$p_0 = E_{total} \div (\tau \times b \times \int_{-l/2}^{+l/2} g(y)dy)$$

b = exposed width, l= exposed length, τ= beam on time. g(y) is the normalised profile. The power falling onto the water supply and return pipes in case of undersized test components is taken into account by the application of a correction factor. This correction factor is derived from measured profiles assuming that the test sections are symmetrical with respect to the beam centre.

2.2 Ion Beam

Roughly 50% of the extracted ion beam is converted into neutral atoms due to charge-changing collisions after acceleration. The beam can be 100% amplitude modulated with a minimum off period of 30 ms and a minimum on period of approximately 3 ms. This modulation has been used to simulate the sweeping of the plasma strike point over the dump plates.

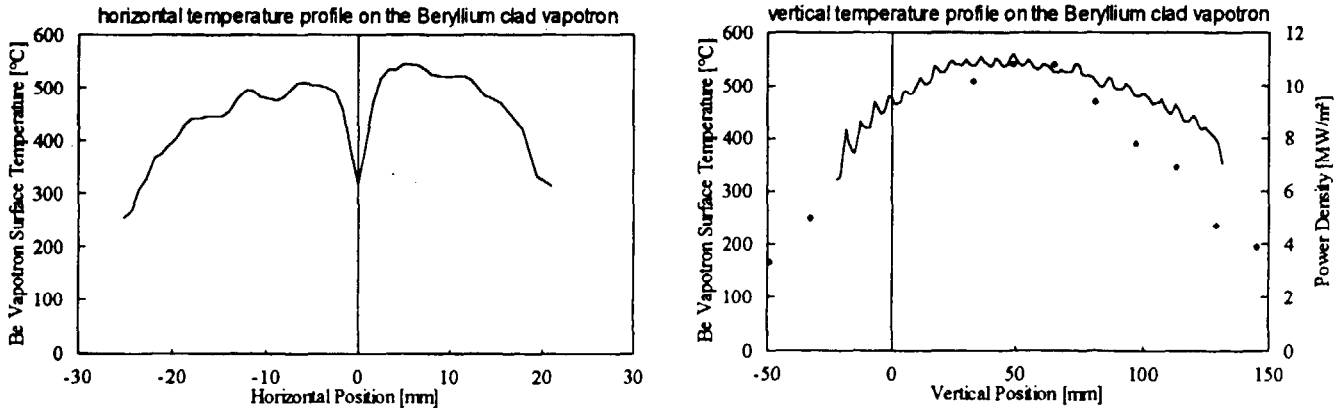

Fig. 3: Horizontal and vertical temperature profiles of two Beryllium test sections during beam on. The horizontal profile clearly shows the gap between the two test sections. The vertical temperature profile (solid line) appears wider than the vertical calorimetric power density profile (dots).

2.2.1 Beam profile

The distance between the beam source and the test section is 7m in the large test facility. The beam has essentially a gaussian shape with a small (30 mm) flat top in the vertical plane and with scraped edges (±75 mm) in the horizontal plane. The 1/e width is of the order of 100 mm. In the Be test rig the distance between beam source and test section is of the order of 2m and the beam profile should have a flat top area determined by the dimensions of the extraction area of the plasma source of 200 x 100 mm^2 (vertical x horizontal). Profiles of the surface temperature measured with the IR imaging systems and inertially measured vertical profiles indicate a more peaked profile than expected from the geometrical parameters (Fig. 3).

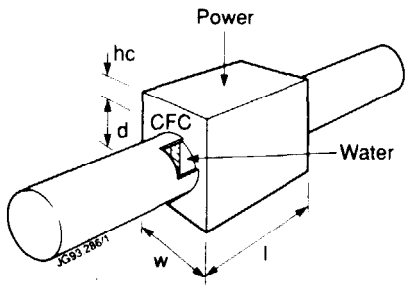

Fig. 4: Monoblock test section.

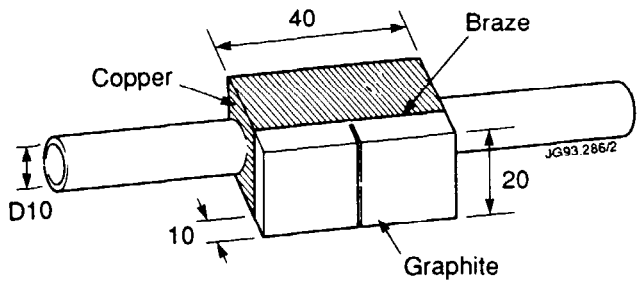

Fig. 5: Flat tile test section. 2 square CFC tiles are brazed to a cooled OFHC copper block (dimensions in mm).

3 TEST SECTIONS

3.1 Actively Cooled Carbon Fibre Composites

Three test sections, supplied by NET, are of the so called monoblock design (solid cubic CFC blocks with a central drilling are brazed onto cooling pipes - Fig. 4). The cooling pipes have an internal swirl ribbon with twist ratio 2 as turbulence promoter. One test section, supplied by Toyo Tanso via JAERI, is of the flat tile design as described in ref[8] (Fig. 5). The main parameters of the test sections are listed in Table 2:

Table 2: Parameters of the CFC monoblock and flat tile test sections.

#	manu-facturer	tile material	tube material	thermal cond. 30°C (W/m/K) parallel / normal	thermal cond. 1000°C (W/m/K) parallel / normal	tile dimensions w x l x h mm x mm x mm	number of tiles	tube diameter D & distance to surface h_c
1	Plansee	SEP N1	TZM	105 / 62	62 / 45	24 x 25 x 27	5	15.9 & 7.1
2	Plansee	A05	TZM	234 / 76	100 / 53	22.2 x 11 x 26.2	10	15.9 & 6.8
3	Ansaldo	CX2002U	Glidcop A125	381 / 215	153 / 93 (900K)	19.3 x 5.8 x 27	17	12.7 & 6.9
4	Toyo Tanso	CX2002U	OFHC copper	381 / 215	153 / 93 (900K)	20 x 20 x 10	2	(flat tile) 11

3.2 Actively Cooled Beryllium Components

Castellated Beryllium tiles are brazed to an actively cooled CuCrZr base with an induction brazing process using InCuSil ABA braze (27.5% Cu, 13% In and 1.25% Ti). The brazing temperature is 730°C for 1 minute. The time

Fig. 6: Test section with Beryllium tiles brazed to CuCrZr vapotron base plates

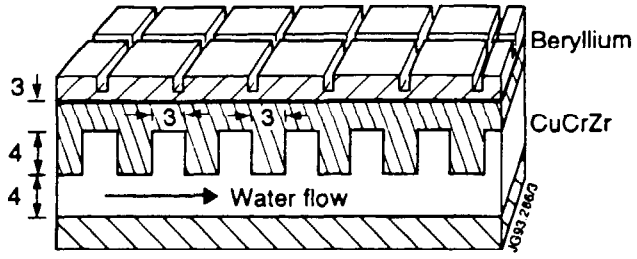

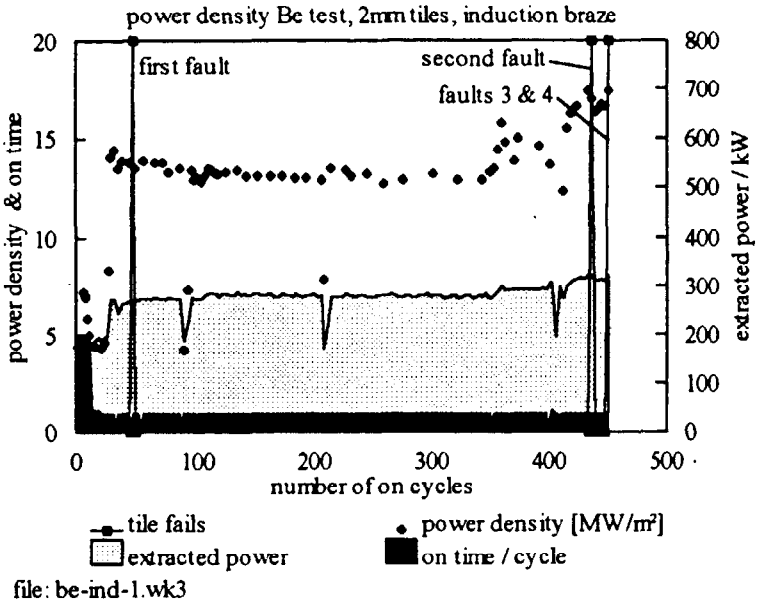

Fig. 7: Test sequence of the Be tile test - 2mm tiles. The dots give the calorimetric power density (left scale), the shaded areas show the beam on time and the extracted beam power.

constant for temperature rise and cool down is 6 °C/s. The heat transfer between the copper base plate and the cooling water is based on the hyper vapotron principle[9]. The test sections have a surface of 500 x 27 mm². The design is shown in Fig. 6. The tile thickness was between 1.5 and 3 mm.

4 TEST RESULTS

4.1 Beryllium Tiles

First individual test sections were tested to define the performance limit of the test section. This was done for 1.5, 2, and 3 mm thick Beryllium tiles all brazed with the same process and castellated in the same way. A typical test sequence is shown in Fig. 7. The test starts with 5 s long unmodulated pulses to set up the beam parameters. Then a change is made to modulated pulses with on/off cycles of 1 s each. After some hundred cycles at constant settings the power density is increased. The tile surface is monitored with a CCD camera and with an IR thermal imaging system. The test is terminated when several hot spots start to develop together or within a few pulses of one another. This is illustrated in Fig. 8.

The test results are given in Table 3 for all three tile thicknesses. The overheating of one or several squares is defined as a fault. All the faults started at the right edge of the test section, where the power density was the highest. In the case of the 1.5 and 2 mm thick tiles the slots stopped the spreading of the melting and the damage was normally confined to the area between neighbouring slots (Fig. 9a). In the case of the 3 mm thick tiles the initial damage was spread over 4 squares and within the next 30 cycles another adjacent square melted (Fig. 9b). The difference in power handling between the three material thickness' was small: tiles with 2mm appeared to be slightly better than those with either 1.5 or 3 mm, but the difference was only of the order of 20% in power density.

Fig. 8: IR. thermogram at the end of a test. Only one test section is installed. Several hot spots are visible at the right edge of the test section

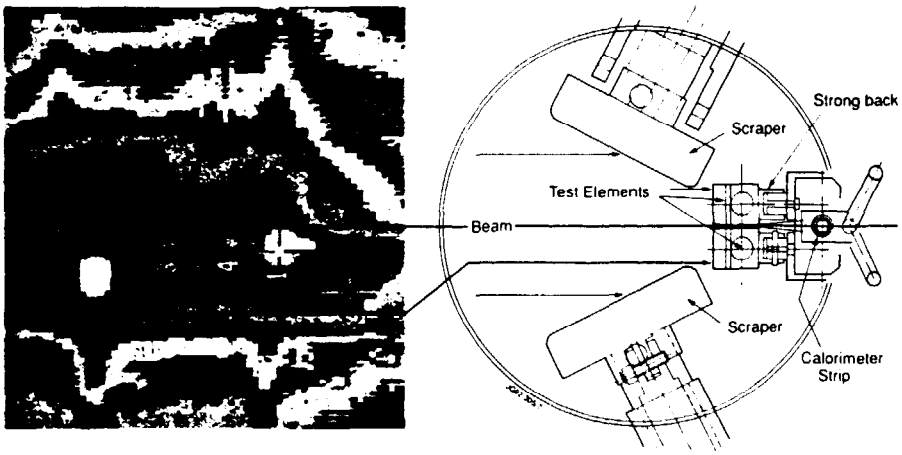

Table 3: Summary of the screening test on Be tiles with 1.5, 2, and 3mm tiles							
fault	cycles to fault	cycles < 10 MW/m²	cycles 10 -12 MW/m²	cycles 12 -14 MW/m²	cycles 14 - 16 MW/m²	cycles 16 - 18 MW/m²	cycles > 18 MW/m²
1.5 mm thick tiles							
1	416	19.3%	37.1%	42.9%	0.7%	0	0
2	554	26	36.3	35.5%	1.7	0.4%	0
2 mm thick tiles							
1	44	79.2%		12.5%	8.3%	0	0
2	436	17.3%		65.5%	9.9%	7.4%	0
3	451	16.8%		65.8%	9.9%	7.5%	0
3mm thick tiles							
1	424	37%	9.2%	50.5%	3.3%	0	0

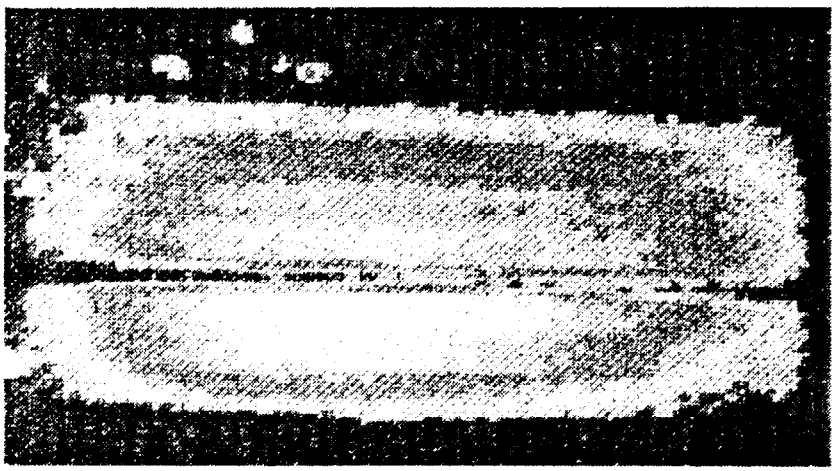

Fig. 10: Temperature distribution on the Beryllium test sections with 2mm tiles during the endurance test. The temperatures are measured within 40 ms after beam off.

Fig. 9: 2 mm (left) and 3 mm (right) Beryllium tiles after the screening test. Melting starts at the right edge and is stopped by the slots. In the case of the 3 mm tile the melting is spread over 5 adjacent squares.

The first fault on the 2 mm thick tile was observed after only 44 cycles and was confined to one or two squares. The next damage only occurred 400 cycles later at a higher power density. We can therefore assume that this first fault revealed a weak area not discovered by the ultrasonic testing.

All the power densities quoted are averaged horizontally over the width of the test section. If we assume, that the surface temperature in Fig. 3 is proportional to power density, the peak power densities at the right edge, where the melting starts, are 15 % above the power density quoted in the table.

Table 4: Test summary of the endurance test on 2mm thick Beryllium tiles			
modulation	**power density in MW/m²**		**number of on cycles**
	average	**peak**	
set-up pulses			32
6s on time	12.2	15.1	73
2s on 1s off	12.5	13.8	307
1s on 1s off	12.8	14.8	552
2.5s on 1s off	12.5	13.8	40
pulses total			1004

4.1.1 Endurance test

Two new test sections were exposed to more than 1000 cycles with an average power density of 12.5 MW/m². The sequence used is listed in Table 4. One 6x6 mm² area well outside the beam centre on the right test section was getting hot from the start of the

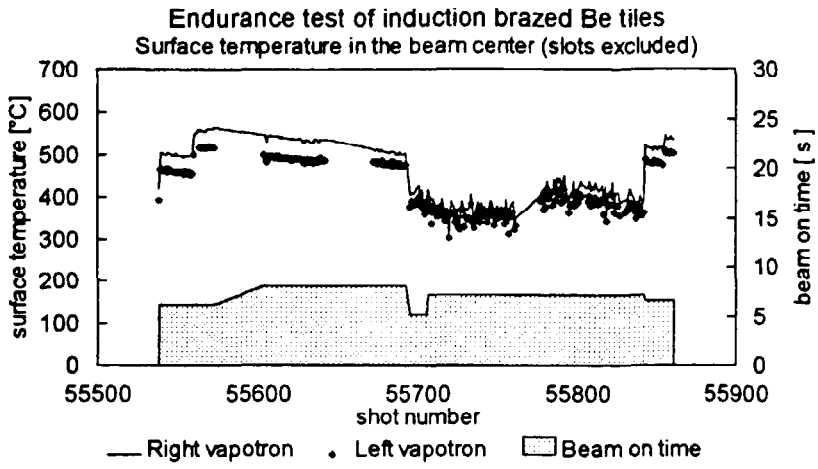

Fig. 11: Temperature history during the Beryllium endurance test. For the different settings the temperature was read at different times during or after the pulse and are therefore at differnt levels. Note: The temperature does not increase during any fixed setting.

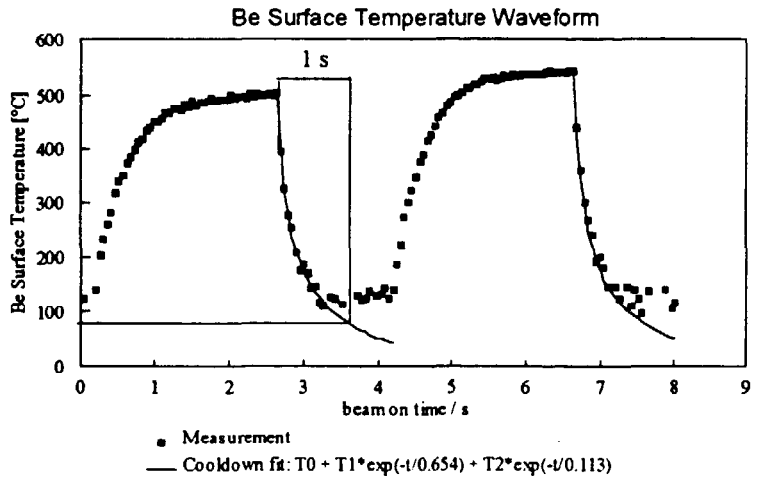

Fig. 12: Time constant of the surface temperature cool down for the Beryllium tile test.

test. Otherwise no deterioration of the tile performance was observed and the surface temperature distribution was uniform (Fig. 10). The surface temperature measurements were taken at fixed times within one scan. Between scans the time of the temperature measurement had to be changed occasionally and this shows up as temperature discontinuity in Fig. 11. However, apart from these discontinuities, there was no increase in temperature during any of the scans. This shows, that there was no deterioration of the tile during the test.

As shown in Table 4, more than 50 % of the cycles were done with one second on time and 1 s off time. 90% of the equilibrium surface temperature was achieved within 1 s of beam on and the tile cooled down to less than 100°C within 1 s of the power being switched off (Fig. 12).

4.2 Flat CFC Tile

The test sequence is detailed in Table 5. Fig. 13 shows CCD camera pictures of the tiles during the cooldown at the beginning of the test (top left) and at the end of the test (bottom right). From the start of the experiment both tiles had adjacent areas with increased temperature (Fig. 13a). No significant change was observed during the first 400 cycles when the power density was varied between 7 and 17 MW/m^2 with a reduced pulse length to keep the surface temperature inside the range of the IR system (1500°C) (Fig. 13b & c). The right tile

Table 5: Test results of the test section with flat CFC tiles

pulse numbers		power density	pulse length	cycles cum.	cum.. on time	comments
from	to	MW/m^2	seconds		seconds	
56514	56525	7	3, 6, 10	11	83	lack of cooling at bottom centre of both tiles
56528	56533	10	10	17	60	as above
56536	56541	11.5	10	23	57	
56545	56560	13	5	39	79	right tile area facing left tile lost cooling
56563	56573	17	1, 2, 2.5	55	22.5	as above
56587	56647	9	2	172	230	as above
56650	56837	13	2.5	412		as above
56840	56879	13	10	454	382	right tile detaches completely

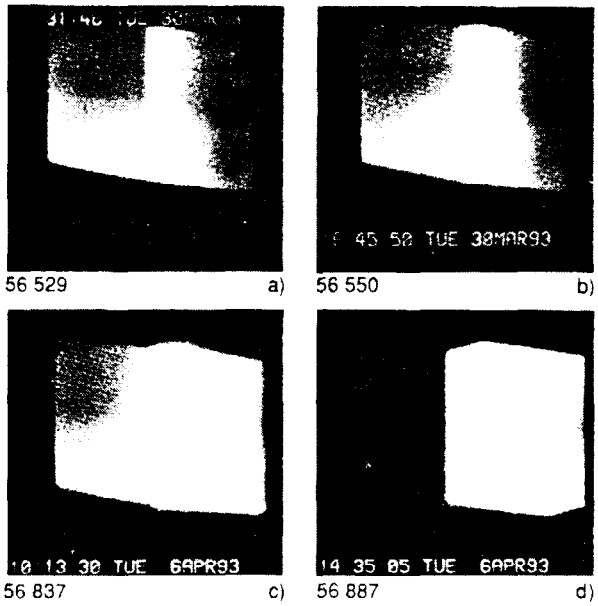

Fig. 13: (left) Glowing of the flat CFC tiles after exposure. The bottom centre is overheated from the start (56529 - less than 20 pulses). 20 pulses later (56550) the left edge of the right tile is hot over the full height. The damage grows over the next 300 cycles (56837) and the tile finally detaches after 30 pulses with 13 MW/m2 and 10 s duration (56887).

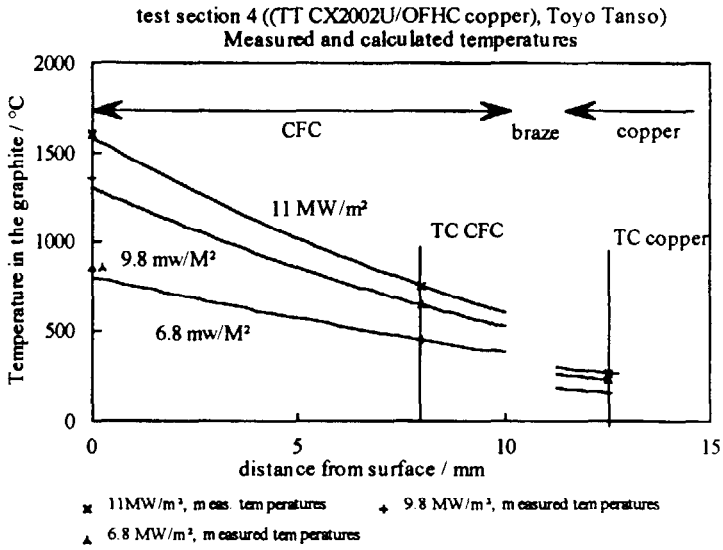

Fig. 14: Temperature in the graphite and copper calculated from measured thermocouple temperatures and power density with CX2002U data using one dimensional heat flow. The surface temperature measured with the IR. system is shown as symbol and agrees well. The middle section, not covered by data points, is the braze with a temperature difference of 200 - 300 °C.

detached completely within some ten pulses at 13 MW/m^2 after the pulse length had been increased to 10 s (Fig. 13d)). The measured surface temperature agreed well with that calculated from the temperature measured with a thermocouple 8 mm below the exposed surface (Fig. 14). The temperature difference across the braze is estimated to be between 200 - 300°C from thermocouple measurements.

4.3 Monoblock CFC Tiles

The three test sections have been tested in pairs and were installed one above each other. The test sections are numbered in table 2 and are quoted with this number , the material combination (CFC/cooling pipe), and the manufacturer. The principal results from the tests can be summarised as follows:

- Section #1 with 5 larger tiles ((SEP N1/TZM),Plansee) showed a regular temperature distribution with a peak temperature above 1500 °C at 15 MW/m^2 (Fig. 15). The three tiles in the centre had been pretested and were slightly hotter than the other two tiles which had not been cycled before. The scanning IR. imaging system used in Fig. 15 does not show the temperature steps from tile to tile which are clearly seen by the CCD camera (Fig. 20).

- Section #2 ((A05/TZM), Plansee) had three tiles (out of 10) with significantly higher temperatures (Fig. 15). The different temperature rise of these tiles at the beginning of the pulse (Fig. 16) indicates that this is caused by the thermal properties of the CFC itself rather than by the braze. The spot location of the temperature measurement in Fig. 16 is indicated in Fig. 15. The higher thermal conductivity of the CFC compared to section #1 does not give lower surface temperatures on all tiles, as Fig. 15 shows.

- Section #3 had 17 small tiles ((Toyo Tanso CX2002U/glidcop), Ansaldo). One the 17 tiles became very hot from the start of the test (Fig. 17). There was also a significant temperature variation amongst the other tiles of this test section. However, the good tiles had considerably lower temperatures than in test sections #1 & 2. It is assumed that

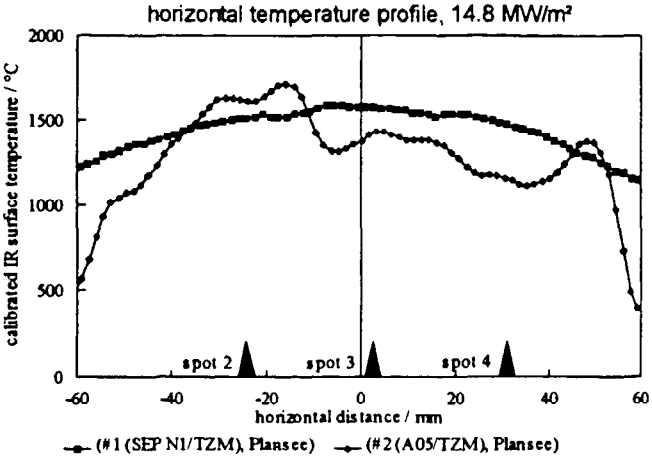

Fig. 15: Comparison of the horizontal temperature profiles for two monoblock CFC sections (both from Plansee. The temperatures are taken at the end of a pulse in which the both sections were being tested simultaneously (identical beam power). Note the large temperature variation in one of the sections.

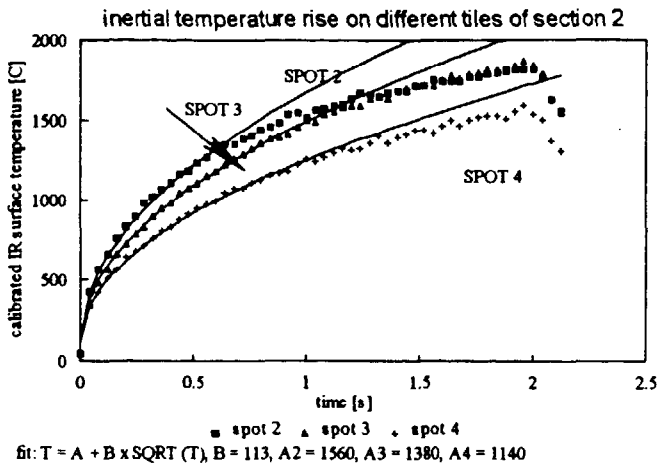

Fig. 16: Temperature rise with exposure for different tiles of the Aerolor A05 test section. The location of the 3 tiles is indicated in Fig. 15. Note that tiles with a higher equilibrium temperature in Fig. 15 have also a faster (inertial) temperature rise in Fig. 16.

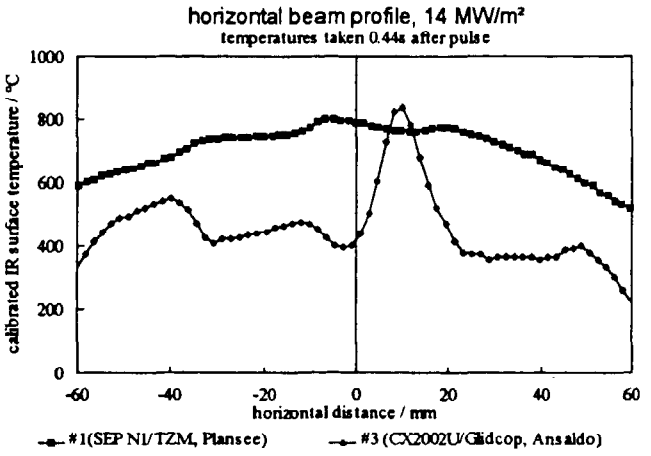

Fig. 17: Horizontal profile of the surface temperature of the monoblock test sections 1 and 3. The temperatures are taken 0.44 s after the pulse and are hence lower than in Fig. 15.

the actual temperature of the hot tile was much higher than the temperatures of section one. This is deduced from the high intensity of visible light emitted from this tile and from the substantial pressure rise observed in the tank (Fig. 19) with this and only this test section. As in the case of test section 2 the higher thermal conductivity of this material does not necessarily result in lower temperatures in comparison with test section 1.

- The surface temperature rose linearly with power density in the case of test sections #1 and #2 (Fig. 18). and was below the calculated temperature at higher power densities, while good agreement is found at lower power density. The same trend is also observed with measured and calculated temperatures at the location of the thermocouples. The fact that the difference is seen with both diagnostics indicates that the measurement is correct and that the thermal properties of the material are better than derived from the material specification at higher temperatures.

- In case of section #3 (Toyo Tanso CX2002U/glidcop), Ansaldo) the tiles were small and the temperature variation across the test section was large. In a scanning measuring system with a finite response time the profile will therefore be smoothed and narrow peaks will be underestimated. This effect will also mask details of the temperature distribution as Fig. 20 shows. The CCD videoprint shows clearly that the centre of the tile, which is closer to the cooling channel, is colder than the edges. Quite in contrast the vertical IR. temperature profile sees a top hat distribution with 5 mm wide falling slopes at the edge instead of the expected peak. Similarly the videoprint in Fig. 20 shows that the rightmost tile of the lower test section is very hot, much hotter than the tile above. Again, this

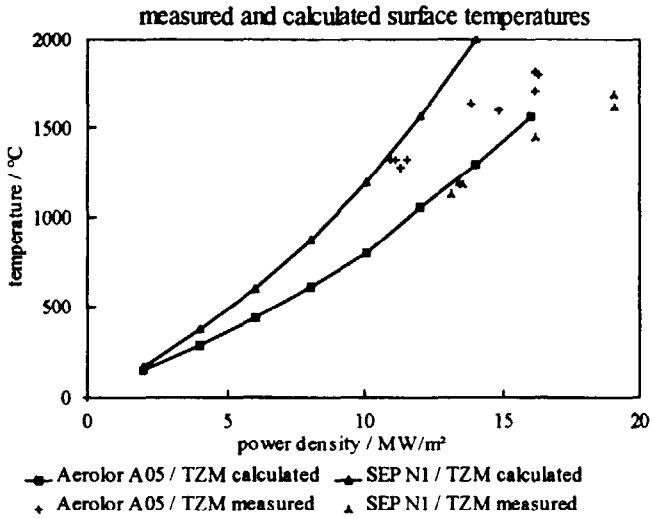

Fig. 18: Surface temperature and thermocouple temperature of test sections 1 & 2. The temperature is taken from good tiles. Within the accuracy the temperature rises linearly with power density and is lower than the calculated temperature both on the surface and for the thermocouple. The linear temperature rise fits with a factor of 114 and 87 °C m²/MW for test sections 1 and 2.

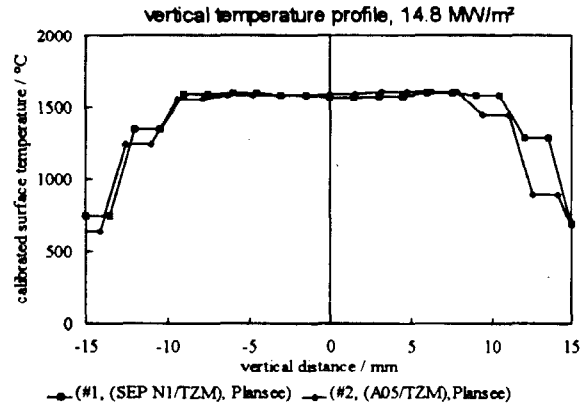

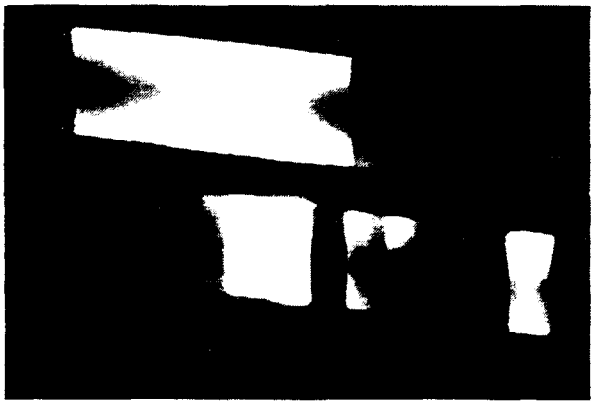

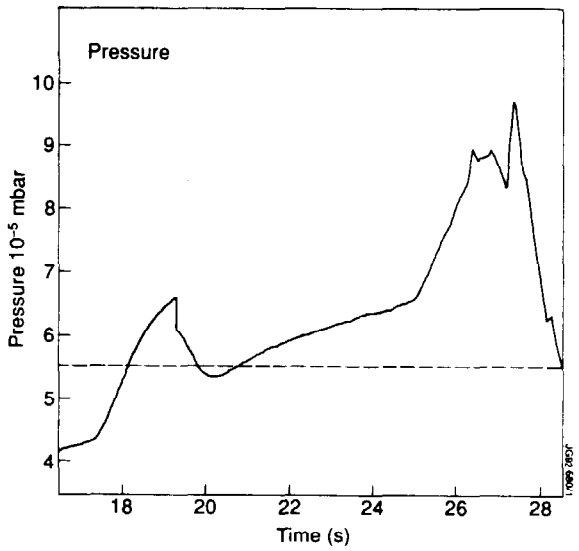

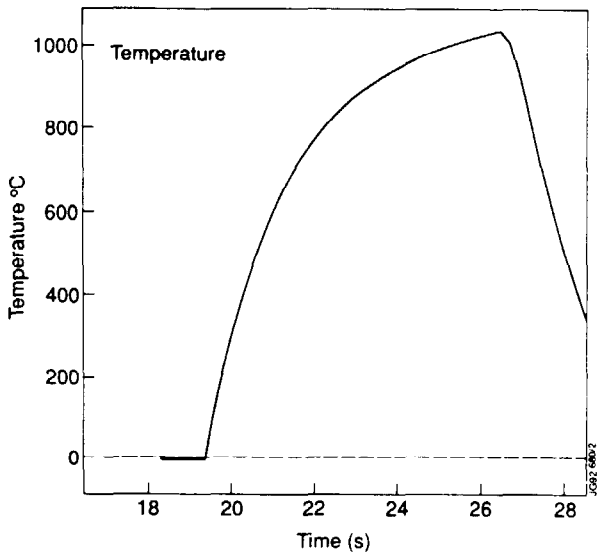

Fig. 19 above: Tank pressure and temperature of a good tile (test #3 (CX2002U/Glidcop, Ansaldo). After 5 s of exposure at 15 MW/m² a sudden pressure rise is observed. The power density of the beam was constant. as the temperature trace proofs.

Fig. 20: (left). View on the monoblock test sections # 1 and 2 with the IR. imaging system (top) and with a CCD camera (bottom). Note: The IR. profile does not resolve the vertical temperature profile on the upper tile (#1) with hotter edges and lower temperatures closer to the cooling channel. The rightmost tile in Fig. 15 (same pulse) has the same temperature as the tile above quite in contrast to the CCD picture

is not resolved by the IR. system which sees similar temperatures for both test sections (Fig. 15). IR. camera and CCD camera view the test sections at an angle of 30^0. The two test sections are installed one above the other with 50 mm spacing in the vertical direction and with the upper test section 50 mm in front of the lower test section in the horizontal plane. The lower test section appears offset to the right in the videoprint, while in reality both sections were centred.

- None of the monoblock tiles showed significant deterioration during the few hundred test pulses with power densities of up to 20 MW/m^2 for long pulses and 30 MW/m^2 for 2s pulses.

- A significant pressure rise could be seen from section #3 (Toyo Tanso CX2002U/glidcop), Ansaldo) at longer pulses (Fig. 19). This pressure increase corresponds to a gas flow of 20 mbl/s, which is more than 3 orders of magnitudes above the flux of fast particles falling onto one tile and is probably caused by sublimation. As stated before this indicates that the tile was much hotter than measured by the IR system.

5 DISCUSSION

5.1 Beryllium Tiles

The performance limit of the Beryllium tiles is between 15 - 17 MW/m^2 and has been confirmed in several tests. The actual local power density at the location of the damage could be as high as 19 MW/m^2. There appears to be a trade off between two dimensional heat flow and stress: If the tile thickness is reduced the stress is reduced but the tile becomes more sensitive to small areas with reduced heat transfer as the heat flow becomes more one dimensional. This is probably also the reason why uncastellated tiles performed better than castellated tiles in previous tests[8]. None of the tiles actually detached and fell off in contrast to previous tests. Beryllium tiles appear to be more sensitive to power density and less sensitive to pulse length. Tiles normally start to fail at the edge and a better design of the edge might increase the limiting power density. Failing tiles melt and will cause exposed leading edges.

5.2 Monoblock CFC Tiles

As in other tests monoblocks are found to be very rigid. The disadvantage of this design is that it might be difficult to avoid leading edges. The actual limit is the tile temperature rather than the mechanical stress from the power density. The temperature limit for graphite surfaces in tokamaks has been calculated to be between 1600 and 2600 ^{0}K, depending on the self sputtering rate. With the tiles tested in this paper this would limit power densities to 15 MW/m^2 if all tiles were perfect and no allowance had to be made for power bursts from the plasma. Note also that the monoblock cooling technique in two test sections shows considerable temperature variation and one tile appears to have significant sublimation at power densities of 15 MW/m^2. From the limited number of sections tested here it appears that there is a trade off between thermal conductivity and suitability for brazing. The section with the worst thermal conductivity shows the most uniform temperature distribution.

5.3 Flat CFC Tiles

As in a previous test the limit is found to be above 10 MW/m^2. The actual limit might be higher if for a tile with perfect heat contact. The design is sensitive to long pulses and tolerates higher power densities for shorter pulses due to the higher heat capacity compared to Beryllium tiles. A surface temperature of 2000 ^{0}K would limit the power density to 11 MW/m^2 with the design used in this test and excluding hot spots. The advantage of this tile design is that larger plates can be fitted with tiles, the disadvantage is the reduced power handling, the high temperature, and the catastrophic failure mode (tiles fall off).

5.4 IR Imaging

If the IR. imaging system does not have sufficient resolution even significant hot spots might not be resolved. This is clearly visible from the comparison of Fig. 15 and 20. In Fig. 20 for example we can clearly see discrete temperature changes from tile to tile on the upper test section which are not visible in the horizontal profile in Fig. 15 and the vertical profile does not show the increased temperature at the edges. The resolution is in this case not limited by the number of pixels as the vertical profile shows. The limit is probably the thermal response time of the detector.

The consequence of this observation is, that hot spots are likely to be overlooked by this technique. This is of particular importance in the case of small tiles and imaging systems with a limited resolution (resolution not large compared to tile dimension).

6 REFERENCES

1) *P-H Rebut, "Magnetic confinement Fusion: Recent Results at JET and Plans for the Future", JET-P(92)21, (preprint of an invited talk 3rd Eur. Part. Acc. Conf., Berlin, Germany, 24th - 28th March 1992.*

2) *M Huguet and the JET Team, "Design of the JET Pumped Divertor", JET-P(91)51, preprint of a paper presented to the 14th Symp. on Fus. Eng., San Diego, USA, 30 Sept. - 3rd Oct. 1991*

3) *R Reichle et. al., "Termination of High Performance Plasmas in JET", paper presented at 34th Annual Meeting of the American Physical Society - Division of Plasma Physics (Seattle, Washington, USA, 16 - 20 November 1992), JET-IR(92)09*

4) *H J Jäckel et. al., "Accountability of the Divertor Power in JET", JET-P(93)37, To be presented to the 20th European Conference on Controlled Fusion and Plasma Physics, Lisbon, Portugal, 26 - 30 July 1993,*

5) *P-H Rebut et. al., "The Key to Iter: the Divertor and the First Wall". To be published in the Proceedings of International Conference on New Ideas in Tokamak Confinement (La Jolla, California, USA, 27 - 29 January 1992) JET-P(93)06*

6) *M Araki et. al., "Thermal Response of bonded CFC/OFHC divertor mock-ups for fusion experimental reactors under large numbers of cyclic heat loads", Journal of Nuclear Science and Technology, 29(9), 901-908, (Sept. 92).*

7) *A Cardella et. al., "Design Manufacturing and Testing of the Monoblock Divertor", Proceedings of the 17th Symposium on Fusion Technology, Rome, 14 - 18 September 1992, (211-215)*

8) *T Matsuda et. al., "Carbon-metal brazing for divertor plates in fusion devices", SPIE Vol. 1739 High Heat Flux Engineering (1992), 157-161*

9) *H D Falter et. al., "Thermal test results of the JET divertor plates", SPIE Vol. 1739 High Heat Flux Engineering (1992), 162-172.*